Scattering Properties of Lunar Dust Analogs

S. Davis[a], J. Marshall[b], D. Richard[a,1], D. Adler[b], B. Adler[b]

[a]NASA Ames Research Center, Moffett Field CA 94035, 650 604 4197,
sanford.s.davis@mail.nasa.gov (Corresponding Author)

[b]SETI Institute, 189 Bernardo Ave, Mountain View, CA 94043

[1]Permanent Address: Lawrence Livermore National Laboratory 7000 East Ave, Livermore, CA

Abstract

A number of space missions are planned to explore the lunar exosphere which may contain a small population of dust particles. The objective of this paper is to present preliminary results from scattering experiments on a suspension of lunar simulants to support one such mission. The intensity of the light scattered from a lunar simulant is measured with a commercial version of the spectrometer used in the forthcoming LADEE mission. Physical properties of the lunar simulant are described along with two similarly-sized reference microspheres. We confirm that micron-sized particles tend to form agglomerates rather than remaining isolated entities and that certain general characteristic of the target particles can be predicted from intensity measurements alone. These results can be used directly to assess general features of the lunar exosphere from LADEE instrument data. Further analysis of particle properties from such remote sensing data will require measurements of polarization signatures.

Keywords

Lunar dust; Mie scattering; Lunar exosphere; Lunar missions

Introduction

Airless bodies in the Solar System outnumber those with viable atmospheres. Missions designed to understand the physical characteristics of asteroids and planetary moons are being planned or are actively underway. The archetypal airless body is the Moon, the subject of numerous missions. The 1970's Apollo project was the primary data source for such airless, crater-impacted bodies, and lunar properties are fully documented based on knowledge gleaned from this and other early space missions in the "Lunar Sourcebook" (Heiken et al., 1991). In particular, the lunar regolith was identified as a continuous distribution of finely grained granular material with many of the particles being sharp or glassy with irregular shapes. The regolith contains grains of all sizes down to submicron as a result of meteorite gardening. The Moon is also subject to bombardment by solar radiation and solar wind (plasma) that induces surface

charging possibly leading to levitation of dust particles. Some indications of this phenomenon were recorded during the Apollo and Ranger missions and are described in the Lunar Sourcebook just cited.

The objective of this work is to develop laboratory data to support observational data from the LADEE mission. One of the lunar data-sets consists of phase functions using remote sensing at points in the lunar exosphere at various latitudes and the current experiments use a spectrometer similar to that used in the mission These results will be helpful in gaining a better understanding of typical particle sizes in the lunar atmosphere and, in particular, an assessment of the aggregation state of these small, irregular, micron-sized particles. Predicted particle sizes will be compared to data from another instrument designed to capture suspended lunar particles.

It is possible that the Moon possesses a thin dust-laden exosphere consisting of these suspended dust grains. The suggestion of dust levitation and transport above the lunar surface derives from the cameras of the early Surveyor and Lunokhod missions which captured images of streaks above the horizon at sunset --the so-called “horizon glow.” This phenomenon is often explained by scattering of sunlight by a cloud of suspended dust particles. The Lunar Ejecta and Meteorites experiment—aboard Apollo 17—recorded dust impacts on its sensors as evidence of surface dust dynamics. This indicated the presence of slow moving highly charged dust particles, particularly at the passage of the day-night terminator. The crew of several Apollo missions observed streamers and glows at spacecraft sunrise which can be explained by sunlight scattering by micron-sized particles above the lunar surface. Based on an analysis of the Surveyor data, Rennilson and Criswell (1974) conclude that the horizon glow is real and caused by backscatter of ~10μm particles.

The interaction of solar wind and radiation with the Moon generates and an electric field associated with a thin Debye sheath. The forces on small dust particles in this environment was investigated in detail by Nitter and Havnes (1992) among others. This early work on the levitation problem was extended by Stubbs et al. (2006). The latter paper predicts that sub-micron particles can be levitated in ballistic trajectories (a “fountain” model) far beyond the Debye sheath to heights of up to 100 km. Thus, the lunar exosphere might possess an extensive vertical profile of dust grains of various sizes that scatter ambient sunlight. Lunar horizon glow remains a subject of interest and recent research extends the modeling to include irregularly shaped particles and polarization properties of the scattered dust (Richard et al., 2011).

The possibility of the Moon possessing a thin dust-laden atmosphere along with the need to document the primitive undisturbed state of the lunar exosphere led to a new lunar mission: the Lunar Atmosphere and Dust Environment Explorer (LADEE) scheduled for launch in 2013 to study the Moon's exospheric dust. One on-board instrument is an ultraviolet- to visual-range spectrometer to measure scattered light intensity from dust grains. The pre-programmed spacecraft trajectory will enable intensity measurements at many positions in the Sun-dust-sensor scattering plane from near forward- to backscatter-directions.

It is recognized that intensity measurements alone are probably not sufficient to fully determine the characteristics of levitated particles using remote sensing technology. In fact, early planetary science investigations identified polarization properties as a viable measurement technique. This parameter was first used by Lyot (1929) to infer properties of the lunar regolith (he correctly concluded that the surface consisted of a powdery material closely resembling terrestrial volcanic ash). Telescopic observations of polarization from the atmosphere of Venus was correlated with scattering theory by Hansen and Arking (1971) and was shown to be a relevant parameter.

Recent laboratory studies using a variety of micron-scale particles to generate particle-laden clouds were reported by Marshall et al. (2011). They found that these clouds tend to be composed of aggregates rather than individual dust grains. It is explained that adhesive forces and sediment inhomogeneity would cause particles to form clumps or aggregates rather than remaining as individual particles (a universal property of dust and powders). Based on these findings they conclude that a dusty lunar exosphere would have an array of aggregates in preference to small individual particles. The sizes and abundances of these populations are unknown and would presumably vary with location on the Moon and distance above the lunar surface. In this paper, we therefore consider the case of light scattering from aggregated particles, but utilize a liquid suspension rather than air. An aqueous suspension can be maintained for extended periods and small van der Waals grain clusters are stable.

The objective of this paper is to present preliminary results from scattering experiments that simulate the function of the LADEE UV-Visual spectrometer in detecting exospheric suspended dust. We first describe the laboratory apparatus and the system used to acquire and process the data. The spectrometer used to measure the scattered signal is a commercial version of the LADEE instrument. The simulant is designated NU-LHT-700-1x and is representative of the lunar highlands. Physical properties of the lunar simulant are described along with two reference scattering targets consisting of 2μm and 8μm borosilicate microspheres. The experimental data are then compared to Mie theory using measured size distributions obtained from SEM images. From the experimental data we found reasonable agreement with theory but the experiment/theory comparison indicated a likely population of aggregated particulates rather than monodispersed material. We conclude that angular intensity measurements alone from the LADEE mission are sufficient to glean general characteristics of the light-scattering particles.

Experiment and Data Reduction

Our goal in this paper is to acquire sufficient laboratory data to aid observations and analysis from the LADEE mission. We focus here on calibration experiments using fine-grained (micron-sized) lunar simulant along with reference microspheres. The lunar simulant is representative of the lunar highlands region and the reference spheres were chosen to bracket the simulant's size range.

1. Experimental Configuration

The scattering experiments were designed to measure the angular phase function from light scattered by lunar dust simulants and to compare these results with theory. We use the Mie theory for comparison since this is the simplest formalism that captures major features of the scattering phase function. It is based on assuming spherical dielectric targets (diameter d) irradiated by an electromagnetic plane wave (wavelength λ). The character of the scattered experimental signal depends on d/λ and this theory will also be used to assess the observational data. Initial reference measurements using borosilicate spheres were used as a validation and calibration tool.

The experimental configuration is shown in Figure 1 and consists of a light source, the target material, and a detector. The experiment is highly automated because fine angular resolution is necessary to fully resolve the scattering signature. The light source is a 5mw red laser emitting at 540 nm. The target particulates are suspended in deionized (DI) water in a 500 ml glass cylinder. The sensor is a small fiber optics probe coupled to a spectrometer (Ocean Optics model QE65000) similar to the ruggedized instrument chosen for the LADEE mission. The laser light source is fixed relative to the target and the rotatable sensor automatically traverses an arc of 180 deg. in about 10 min. There is a small range of unusable angles around 0 (forwardscatter) and 180 deg. (backscatter) that is contaminated by either the incident beam or probe interference. The light source is held at the same relative height as the sensor and the target's container is canted very slightly upwards (~ 5 degrees) to reduce reflections from the glass tube itself (by so doing, wall reflections are deflected out of the observation plane).

Both rotational motion and data collection are controlled using a LabView based computer program configured specifically for this experiment. Data acquisition/processing consist of 3 steps: (1) A reference data set is collected using only DI water in the glass cylinder over the entire angular range. (2) The target material is added and a second data set is acquired with all parameters remaining constant. (3) These data sets are differenced to capture the scattered signal itself. In a typical case data is acquired in 1-degree increments except for a small region in the forward and backward directions. One of the spectrometer parameters is the integration time that is the time over which the 540 nm wavelength bin collects sample data. This time was varied between 10ms and 1s. The effect of particle sedimentation was investigated by repeating the experiment after selected time intervals. After each such experiment particle samples were dried and collected on micron filter paper. These samples were examined by scanning electron microscope to determine the size distribution at selected time intervals. They were also correlated with the results of Stokes' settling calculations based on the elapsed time from the start of each experiment.

2. Preparation of the target material and experimental protocol

The borosilicate spheres are nominally 2μm and 8μm in diameter (Thermo Scientific Duke Standards 9000 Series Glass Particles, Part numbers 9002 and 9008). The published size specifications are 2.± 0.4 and 8.1±0.5 with an index of refraction of 1.56 at standard conditions.

The lunar simulant is that designated NU-LHT-700-1x which is a lunar highlands analog and representative of finer grained material (Stoesser et al., 2008).

The DI water was used as a suspension medium and 0.1 g of either the lunar simulant or 8μm spheres was suspended in 500 ml of the liquid. A smaller amount of 2μm particles were used since a full 0.1g mass of solute caused the solution to become visually cloudy. The mean distance between particles in all three cases was about 100μm which allowed single-point scattering. The dry particles in their original containers were clearly aggregated and in each case the solution was ultrasonically dispersed for about 10 minutes to mostly de-aggregate the particles. The phase function was determined at a series of time lags to allow sedimentation of the heavier particles that would presumably affect the scattering pattern. This was true for the 8 micron particles but not true for the two other samples since their small size would ensure suspension for very long time intervals (owing to Brownian motion). In fact, for the case of the lunar simulant it was found that the mean particle size increased slightly due to agglomeration. Table 1 depicts the range of sedimentation times used for the three considered target materials.

Table 1. Experimental Scattering Test Matrix

Target	t=0 hrs.	t=1 hr.	t=6 hr.	t=24 hrs.
2μm microspheres	X	X	-	-
8μm microspheres	X	X	-	-
Lunar simulant	X	X	X	X

3. Some features of the experimental data

Some clues regarding the size of the lunar simulant from scattering data can be gleaned from the raw experimental data itself. In Figure 2 phase distributions are indicated for each of the three targets. In each case the relative intensities are accurate, but the scale is calibrated in arbitrary units – viz., spectrometer-based digital counts. The larger particles scatter most energy which is almost three orders of magnitudes higher than the lunar simulant.

Scattered light from a solitary micron-sized particle at 540 nm would have a rippled appearance (c.f. Davis and Schweiger (2002) p 168 for an experimental example). Here, the size parameter based on particle radius ($ka = 2\pi a / \lambda$) is about 10 and puts the scattered signal beyond simple Rayleigh theory and into the realm of classical Mie scattering. The forward lobe (scattering angles < 90 deg.) dominates most of the energy and there is about a 3 order intensity reduction beyond 90 deg. The irregular shape of the lower level signal reflects either noise or some complex feature of the signature; a common characteristic of all the traces is the upswing at large scattering angles. Even from these raw spectrometer data, definite conclusions can be drawn. The slope of the scattering diagram below 90 deg. is slightly different with the two sphere sizes. The lunar simulant slope is very close to that of the 2μm spheres. Thus, it can be concluded that the mean particle size of the lunar simulant is around 2μm.

Next, some of the target material was isolated from solution (Figure 3) and its size quantified by SEM. The left panel indicates that the microspheres are not uniformly sized, but are size-distributed with a variance consistent with the manufacturer's specifications. The lunar simulant consists of irregularly shaped particles with faceted surfaces. These are quite different from the classical case of atmospheric scattering from aerosols where the particles are generally spherical. This morphology is typical of material on dry, airless solar system bodies. In this study these multi-faceted particles are assumed spherical for comparison with Mie theory.

A size distribution for each particle type was measured in two ways. First, the images were examined particle-by-particle with the lunar simulant considered to be small ellipses. (The images used for quantitative analysis had well-spaced particles.) An equivalent diameter d was computed from the semi-major and semi-minor axes a,b by $2\sqrt{ab}$. The resulting size distributions were spot-checked using an edge detecting image processing algorithm where individual particles were encased by primitive circles or ellipses. The manual and image-processed data were consistent with one another.

The method used to quantify the size distributions are shown in Figure 4. It is based on quantifying the frequency distribution function since is easier to approximate a monotonically increasing function than one having a local maxima. First the individual "frequency bins" of sizes were summed over all smaller sizes to obtain points on an empirical frequency distribution function ranging from 0 (no particles smaller) to 1 (all particles smaller). Next integrate a normally distributed size frequency $f(d)$ of unit area to obtain the frequency distribution function $F(d) = \int_0^d f(x)dx$. $F(d)$ is an Error function with free parameters that best fits the data with the constraints that $F(0) = 0, F(\infty) = 1$ This curve (solid line) along with the data (symbols) are shown in the figure along with the computed frequency distribution function (dashed). The data fit for the spherical particles is quite good indicating for a population of variable diameter spheres centered on 2 μm. The lunar simulant however is not as well represented by an error function since there is a consistent deviation in the comparison. The actual size distribution is clearly asymmetric with a bias towards smaller particles. Considering the wide range of particle shapes involved and the use of a sphere-based scattering theory, the best-fit error function was adopted here to characterize a "mean" particle diameter. More refined fitting curves will be used with non-spherical scattering theories. Results from the current size analysis are shown in Figures 5 and 6 for the complete set of spheres and lunar simulants respectively. In each case the distributions are normalized to unit areas so broader distributions will have lower peak values.

The size-distribution data in Figure 5(a) shows contrasting sedimentation behavior for the two spheres. Smaller particles retain similar means and variances after one hour. This indicates that these particles remain in suspension. The larger particles show a significant drop in mean values after one hour. These data indicate that the heavier particles are prone to sedimentation. This effect was investigated using a simple settling formula where gravity is opposed by Stokes drag

(here the Reynolds number is in the appropriate range) and buoyancy. The settling velocity is computed and the time required for grains to settle a distance of half of the cylinder height (~ 3.25 cm) was computed. Predicted settling times are indicated in Table 2 for a range of particle diameter

Table 2. Settling Times for Various Sized Particles	
size, μm	T, settling time, hrs.
2	6.7
4	1.6
6	0.75
8	0.42
10	0.26
15	0.11

This simple calculation clearly shows that after one hour particles whose diameter is greater than about 5μm can be efficiently removed from the scattering volume while smaller particles will remain in solution for much longer times. This is consistent with the distributions in Figure 5(a).

The effect of these size distributions on the phase function is indicated in Figure 5(b) using Mie theory. The calculation uses a relative index of refraction for silicates in water that is 1.56/1.31 = 1.19 and an incident wavelength of .540μm (green laser light). Computation of the scattering diagram for a mixed size distribution follows standard procedures (Hansen and Travis, 1974). The theoretical intensity ratio is a smooth function of scattering angle unlike individual spheres that have a complex rippled appearance. Unfortunately, micron-sized distributions radiated by visible light do not have unique features over a range of mean values. The only obvious trend is toward higher intensities with larger particles. Other phase function trends are the appearance of an upsweep (the glory) near 180 deg. and the rainbow near 120 deg.

The lunar simulant distributions are quite different. At the initial instant (Figure 6(a)) the mean diameter is about 3μm which confirms the conclusion drawn from Figure 2. However, the mean first decreases to about 1.5μm and then increases steadily to 4.5μm after 24 hrs.. The lunar samples were subject to ultrasonic dispersal for 10 min. prior to the experiment and this process probably separated the sample into its smaller constituents but the tail of the t=0 case contained some larger particles and these may have been removed from the scattering volume at t = 1 hr. At longer times many of the irregularly shaped particles must have coagulated. This clumping effect increased both mean size and dispersion of the particle sizes. This hypothesis will be tested

by comparing the experimental scattering data with Mie theory using these measured size distributions as input parameters.

The theoretical phase functions in Figure 6(b) also show a consistently increasing intensity with mean particle size. A feature of interest is the change in slope for forward scattering. This slope variation was used to advantage in Figure 2 to estimate the mean diameter. Other features are difficult to ascertain, but comparisons with experimental data will show that certain characteristics can be extracted from the measurements.

Discussion

The borosilicate microspheres are consistent with Mie theory assumptions while the lunar simulants may not since the population consists of irregularly-shaped particles. The morphology of the particle types were contrasted in Figure 3. Additional investigations are needed to assess the effect of irregular particles, especially those related to the lunar material (and analogs). It is expected that a significant effect of these multi-faceted particles would be a tendency to form particle aggregates.

Particle distributions are required input parameters since single-sized particles (a “delta-function” size distribution) induce phase functions with a resonance effect (multiple ripples) that is difficult to achieve unless a single particle is used as a target. Representative size distributions and phase functions for the spherical targets were presented in Figures 5 and 6. The four microsphere experiments (two sizes and two settling times) are compared with Mie theory in the following paragraphs. In all cases comparisons were made by scaling the theoretical intensity at 40 deg to the experimental data which are expressed as spectrometer digital counts

Figure 7 compares the experimental data for the 2μm microspheres with Mie theory. The thin line is the raw experimental data and the dashed line is a theoretical calculation using the appropriate size distribution from Figure 5. Generally reasonable agreement is shown except in the low intensity region beyond 90 deg. One feature that is missing in both panels is the pronounced upsweep near 180 deg (as mentioned previously, the container was canted to avoid reflections). Also, no evidence is found of a peak at 120 deg (the “rainbow”) predicted by the Mie theory. The rainbow feature depends on phase-locked internal reflections in the target and it is expected that minimal damping would suppress this effect (Bauer, 1964). In any event, it is difficult to isolate this particular characteristic since the signal is quite noisy for scattering angles greater than 90 deg. A backscatter upsweep (the “glory”) appears in all cases and is more pronounced in the experimental data. The upsweep quality of the phase function may be explained by the presence of a small quantity of larger particles in the scattering volume as described in the following paragraph.

The likelihood of having a simple unimodal size distribution with such particles is small. Experience with dust clouds (Marshall et al., 2011) indicates that a bimodal distribution is more likely since single particles in the micron or sub-micron range tend to from agglomerates.

Similar behavior is expected with small particles in solution. Physical examples can be found in studies of dust grains in the solar nebula where agglomeration of submicron particles is a major driver of the planet formation processes as described by, for example, Dominik et al. (2007). Even though the particles in solution were acoustically de-agglomerated for about 10 min. some residual clumps must exist. Figure 7 is augmented with another calculation where a 2% population of 10μm spheres is added. This is shown by the heavy line. The addition of larger particles indicates a marked upswing in backscattering that is not present using the basic unimodal size distribution. This indicates the presence of a small population of larger sized particles, probably agglomerations. The exact size and conformation is unknown. Comparisons after one hour show a similar trend and indicate that the initial particle population has remained relatively constant. Even though the backscatter agreement is not exact, the qualitative effect has been captured. Note that adding the 10 μm sphere reveals the phase-locked rainbow feature.

Considering the larger 8μm spheres (Figure 8), the fit is reasonable and the experimental data includes the backscatter upsweep feature. However, after one hour of settling some particles must have settled (removed from the scattering volume) and the noise fraction has increased. In general the overall agreement is not as good for these larger particles. In summary, scattering by microspheres in the range 1-10 μm is probably a good representation of that expected in the case of lunar dust and encompasses a range of sizes where the agglomeration effect plays a role.

Based on Figure 2 the lunar simulant is sized between 2 and 8 μm. The irregular shape structure (Figure 3) makes agglomeration a more efficient process and this behavior is investigated using the scattering data. Figure 6 shows that the mean size decreases after one hour (indicating some sedimentation), but there is a clear trend towards increasing mean at larger times. The particles seem to be widely dispersed after 24 hrs. with a 4.5 μm mean. This large dispersion indicates that some portion of the population consists of agglomerated particles.

The experimental phase functions for these four cases are compared in Figure 9 to Mie theory using size distributions from Figure 6. The relative index of refraction is the silicate value of 1.19 and the wavelength is .540μm. Agreement with the basic Mie theory is reasonable considering the shape evolution. The basic theory shows good agreement in the forward scattering direction, but fair to poor agreement in the backscatter region. Additional calculations using a 10% fraction of 10μm spheres does not make a significant difference. One interpretation from Figure 9(b) (after one hour) is that as the larger particles are removed from the scattering volume (decreasing mean) their influence wanes and the upsweep near 180 deg. is eliminated. At larger times the size distribution broadens and scattering from the developing agglomerates induces the backscatter to increase. In this case we would conclude that aggregating particles are the cause.

With respect to the relative magnitudes of the lunar simulant scattering data, they generally conform to Mie theory predictions. That is, in order of increasing mean values in panels (b), (c), (a) the intensity increases in accordance with theory. After 24 hrs. the intensity is lower even though both the mean and the dispersion are higher. The probable cause is sedimentation and a

reduction of the solute number density since this is a larger time than any of the entries in Table 2.

Conclusions

Light scattered from an aqueous suspension of lunar simulants and reference microspheres was investigated in a laboratory-scale experiment. The objective was to characterize the phase functions for the range of particle sizes to be expected in the lunar exosphere. Results of this initial study indicate that a collection of particles in this size range, at the concentrations present in the aqueous solution, would not remain isolated entities but would tend to accumulate into small aggregates. Further detailed (and quite challenging) studies are needed to trace the evolution of these structures. These clusters will be very porous and would require the inclusion of damping terms in the index of refraction parameter.

It is expected that measured properties of the scattering signature would be similar for particles lofted into the lunar exosphere. The lunar exosphere is so rarified that single scattering theory (e.g. Mie theory) should be sufficient to determine first-order size distributions of existing particulates and/or agglomerates. There is good reason, however, to expect that the dust lofted into the exosphere is already in the form of small aggregates (Marshall, 2012; Marshall et al., 2011) and would not require aggregation during suspension. The actual dust lofting mechanism is unknown, but popularly attributed to electrostatic forces (Heiken et al., 1991). These electrostatic forces result from solar radiation and solar wind (plasma) but they also generate repulsion between particles because all particles are like-charged. On the other hand, adhesive (dipolar) forces resulting from contact electrification at grain junctions will work to counter monopolar repulsion. It can also be shown by analysis that the van der Waals cohesive force for dust on the Moon is orders of magnitude larger than any likely electrostatic repulsion force.

Further studies are needed to clarify a number of issues regarding both laboratory results and the actual lunar environment. First, the basic Mie theory phase functions are not sufficiently unique to identify specific particle sizes in the 0.5-10 micron range. It is necessary to supplement the analysis with polarization signatures and even to consider the full set of Stokes parameters at each scattering angle. Secondly, the theory needs to be augmented for non-spherical particle types. In addition to the base literature on non-spherical particles (Mishchenko et al., 2000) a number of new computations on polarization properties of irregular particles is now available (Richard et al., 2011). These theoretical approaches will be used in future investigations.

Solar system missions currently underway to study the lunar exosphere and others planned for nearby asteroids will certainly expand our knowledge of the dusty environment surrounding airless bodies. These findings, coupled with laboratory studies guided by these missions, will greatly expand the knowledge base concerning the particle populations in this very large class of extraterrestrial, waterless, and impact-cratered objects. With respect to the LADEE mission, the existing planned instrumentation coupled with a high angular resolution scattering intensity

measurement should be able to ascertain whether or not the lunar exosphere contains high altitude dust grains. In particular these results should (1) Enable a better understanding of lunar particulates from the measured signatures, (2) Quantify expected scattering phase functions for aggregated states, (3) Use measured phase functions from known particles to assess observations from both remote sensing and particle-capturing instrumentation on the LADEE spacecraft, and (4) Support acquired spectrometer data sets during sweeps to determine altitude dependent size distributions.

References

Bauer, E., 1964. The Scattering of Infrared Radiation from Clouds. Applied Optics 3, 197-202.

Davis, E.J., Schweiger, G., 2002. The Airborne Microparticle: Its Physics, Chemistry, Optics and Transport Phenomena. Springer-Verlag, Berlin Heidelberg New York.

Dominik, C., Blum, J., Cuzzi, J.N., Wurm, G., 2007. Growth of Dust as the Initial Step Toward Planet Formation, In: Reipurth, B., Jewitt, D., Keil, K. (Eds.), Protostars and Planets V. University of Arizona Press, Tucson, AZ, pp. 783-800.

Hansen, J., Arking, A., 1971. Clouds of Venus: Evidence for Their Nature. Science 171, 669-672.

Hansen, J., Travis, L., 1974. Light Scattering in Planetary Atmospheres. Space Science Reviews 16, 527-610.

Heiken, G.H., Vaniman, D.T., French, B.M., 1991. Lunar Sourcbook, A User's Guide to the Moon. Cambridge Univ Press, New York.

Lyot, B., 1929. Recherches sur la polarisation de la lumiere des planetes et de queldues substances terrestres. Ann. Obs. Meudon 8, 1.

Marshall, J., 2012. Entrainment of Cohesive Particulates in Aeolean and Airless Environments. (to be submitted).

Marshall, J., Richard, D., Davis, S., 2011. Electrical stress and strain in lunar regolith simulants. Planetary and Space Science 59, 1744-1748.

Mishchenko, M., Hovenier, J.W., Travis, L., 2000. Light Scattering by Nonspherical Particles. Academic Press, San Diego.

Nitter, T., Havnes, O., 1992. Dynamics of Dust in a Plasma Sheath and Injection of Dust into the Plasma Sheath above Moon and asteroidal surfaces. Earth, Moon and Planets 56, 7-34.

Rennilson, J.J., Criswell, D.R., 1974. Surveyor observations of Lunar Horizon Glow. The Moon 10, 121-142.

Richard, D.T., Glenar, D.A., Stubbs, T.J., Davis, S.S., Colaprete, A., 2011. Light scattering by complex particles in the Moon's exosphere: Toward a taxonomy of models for the realistic simulation of the scattering behavior of lunar dust. Planetary and Space Science 59, 1804-1814.

Stoesser, D.B., Wilson, S.A., Fikes, J., McLemore, C., Rickman, D., 2008. Development of lunar highland regolith simulants. Geochim. Cosmochim. Acta 72, A902.

Stubbs, T., Vondrak, R., Farrell, W., 2006. A dynamic fountain model for lunar dust. Advances in Space Research 37, 59-66.

Figures

Figure 1: Experimental Configuration showing incident beam, traversing sensor, and target material in suspension.

Figure 2. Experimental scattering diagram for three target materials at t = 0 hrs. The features are typical of a size-distributed scattering source in this range of particle size to wavelength ratio.

Figure 3. Scanning electron microscope images of concentrated particles at 5000X magnification. Left panel: Nominally 2μm microspheres. Right panel: Lunar simulant.

Figure 4. Conversion of image processed data (symbols) to an approximate size distribution (dashed) using the frequency distribution function (solid) as an intermediate step

Figure 5. (a) Measured size distributions for 2μm and 8μm spherical test particles showing evolution of size distributions after one hour. (b) Phase function computation using Mie theory.

Figure 6. (a) Measured size distributions for the lunar simulant. Distributions are shown at four sedimentation times to 24 hours. (b) Phase function computation using Mie theory.

Figure 7. Scattering diagrams for 2μm spheres compared with Mie theory. Thin Line: Experimental data. Dashed Line: Mie Theory using size distribution. Thick Solid Line: Mie Theory with a 3% population of 10μm spheres. (a) Initial Instant; (b) One hour settling time

Figure 8. Scattering diagrams for 8μ spheres compared with Mie theory. Thin Line: Experimental data. Dashed Line: Mie Theory using size distribution. Thick Solid Line: Mie Theory with a 3% population of 10μm spheres. (a) Initial Instant; (b) One hour settling time

Figure 9. Scattering diagram for lunar simulant. Thin Line: Experimental data. Dashed Line: Mie theory using size distributions from Figure 5. Solid Line: Mie th

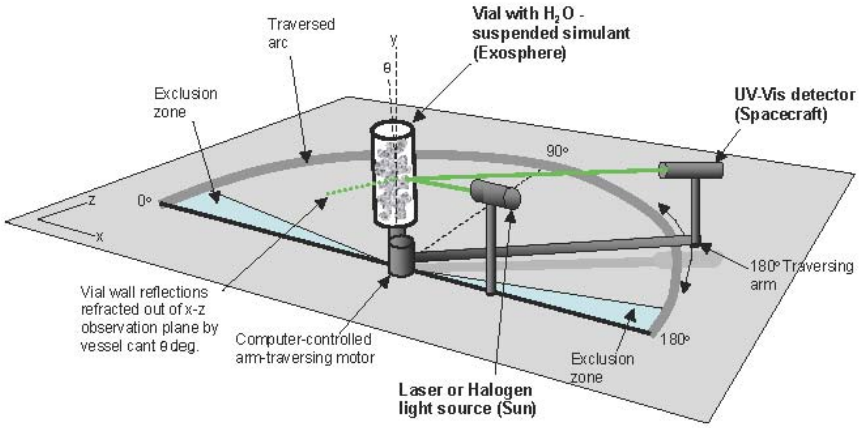

Figure 1

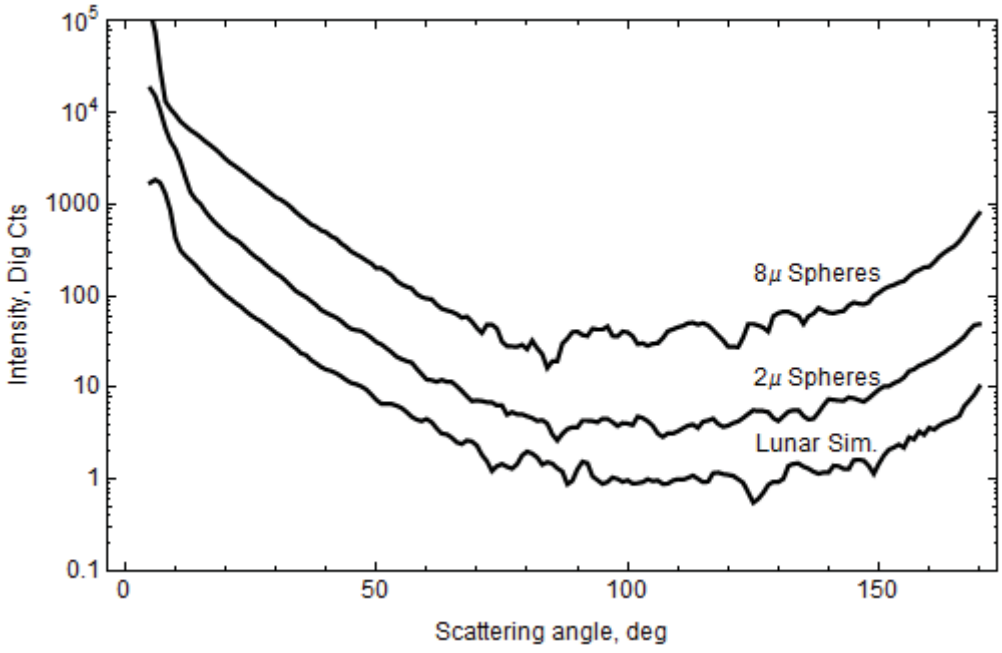

Figure 2

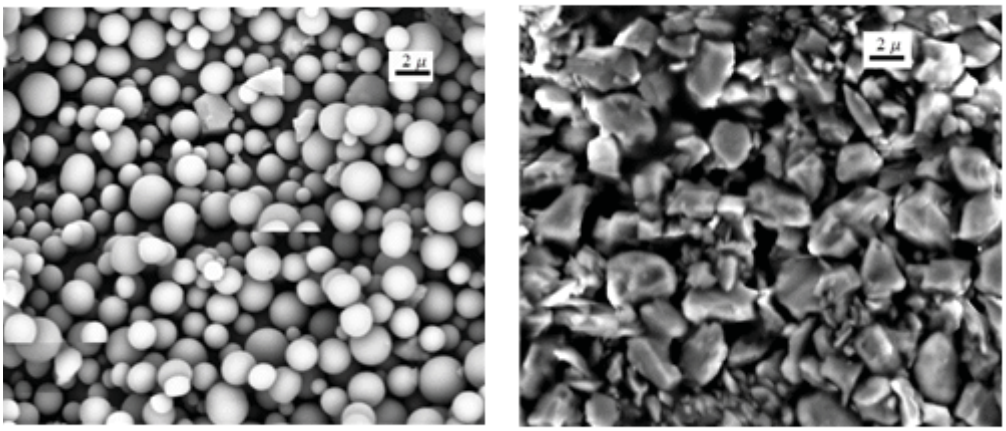

Figure 3

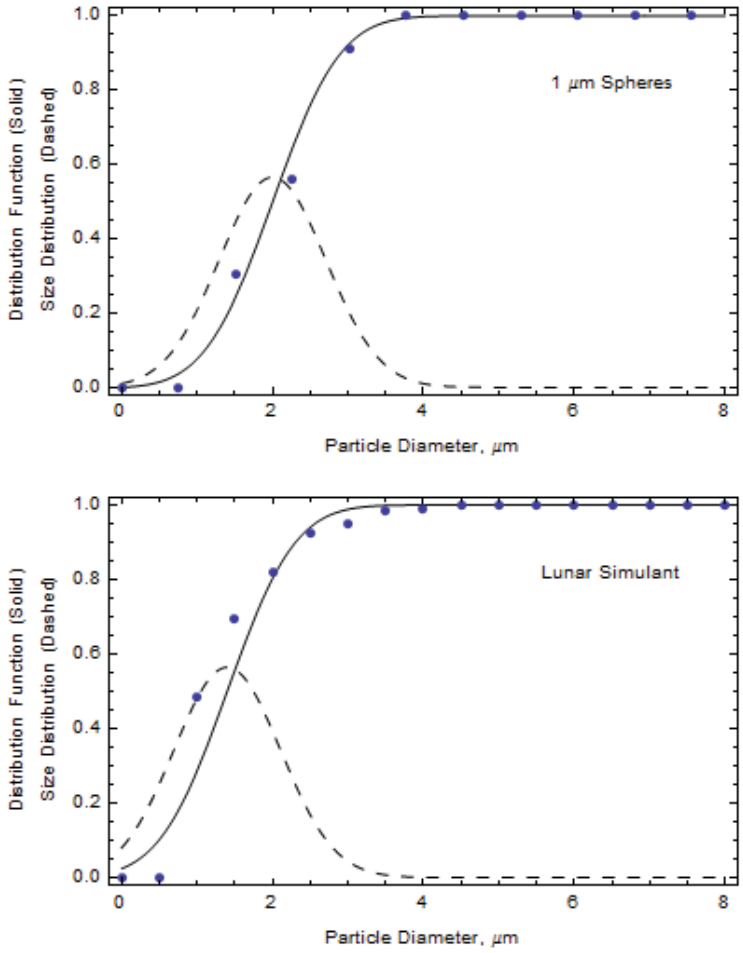

Figure 4

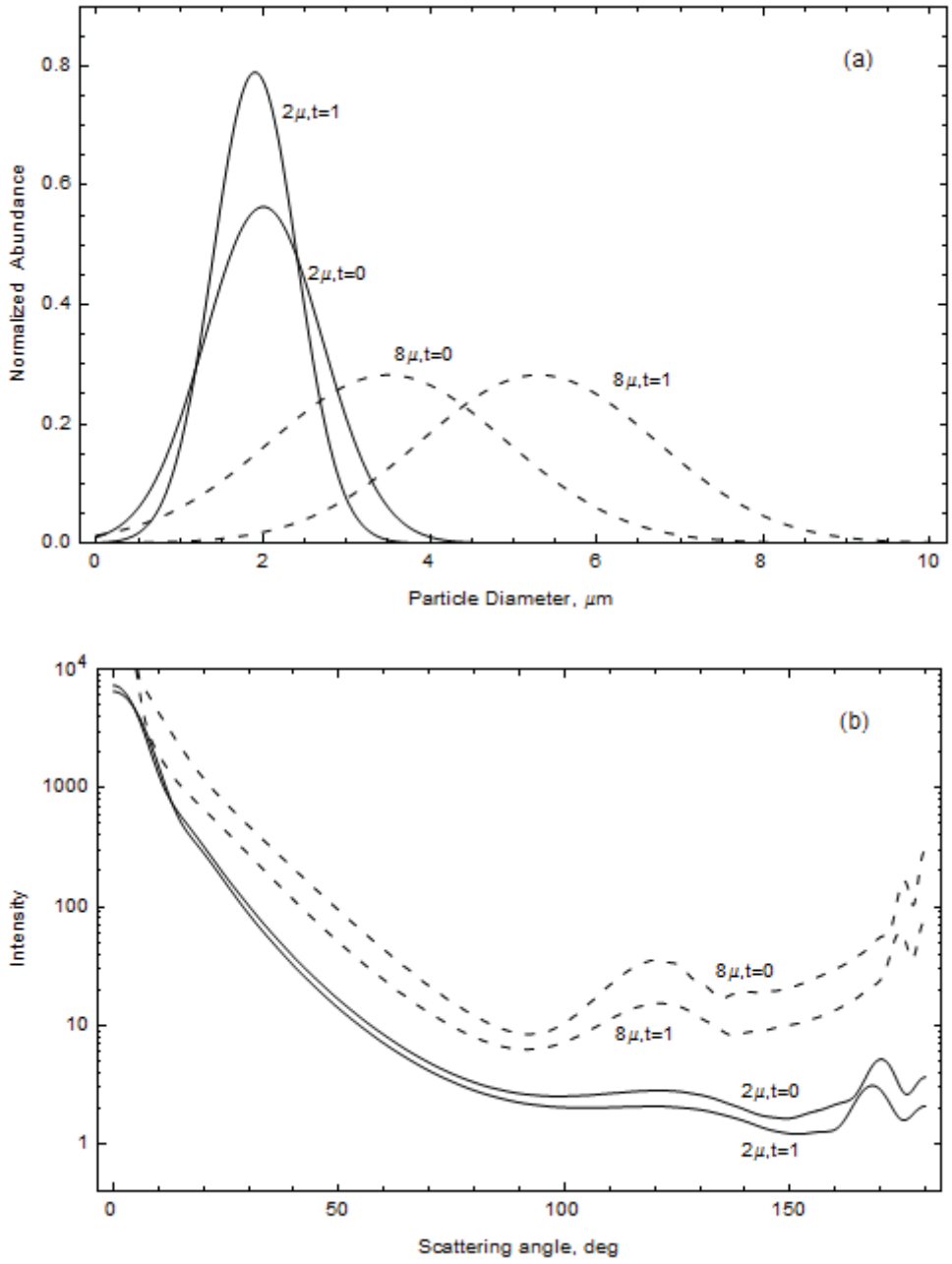
(a)
Normalized Abundance
Particle Diameter, μm
2μ,t=1
2μ,t=0
8μ,t=0
8μ,t=1
0.0
0.2
0.4
0.6
0.8
0
2
4
6
8
10
(b)
Intensity
Scattering angle, deg
8μ,t=0
8μ,t=1
2μ,t=0
2μ,t=1
1
10
100
1000
10^4
0
50
100
150

Figure 5

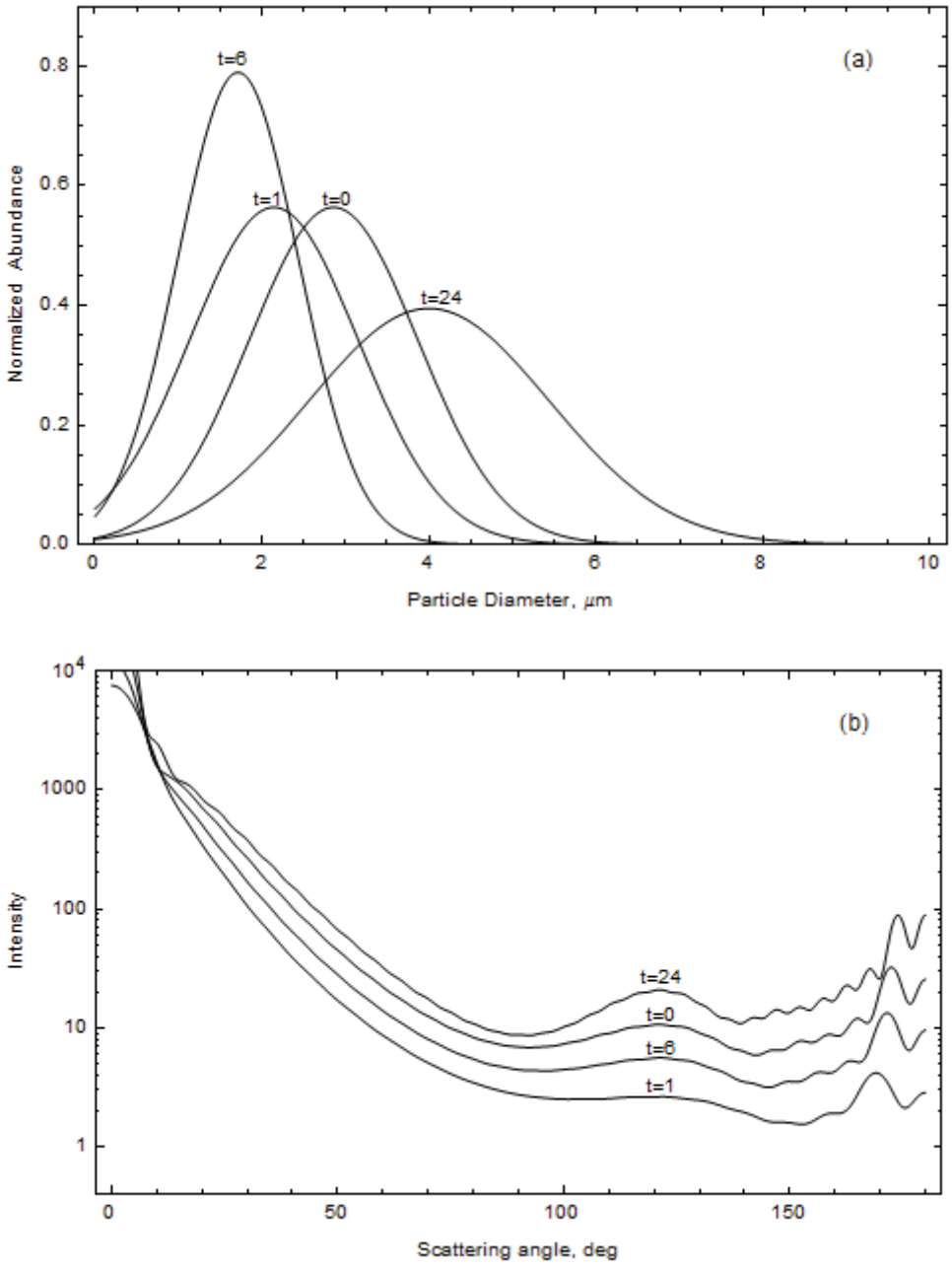
(a)
t=6
t=1
t=0
t=24
Normalized Abundance
Particle Diameter, μm
(b)
t=24
t=0
t=6
t=1
Intensity
Scattering angle, deg

Figure 6

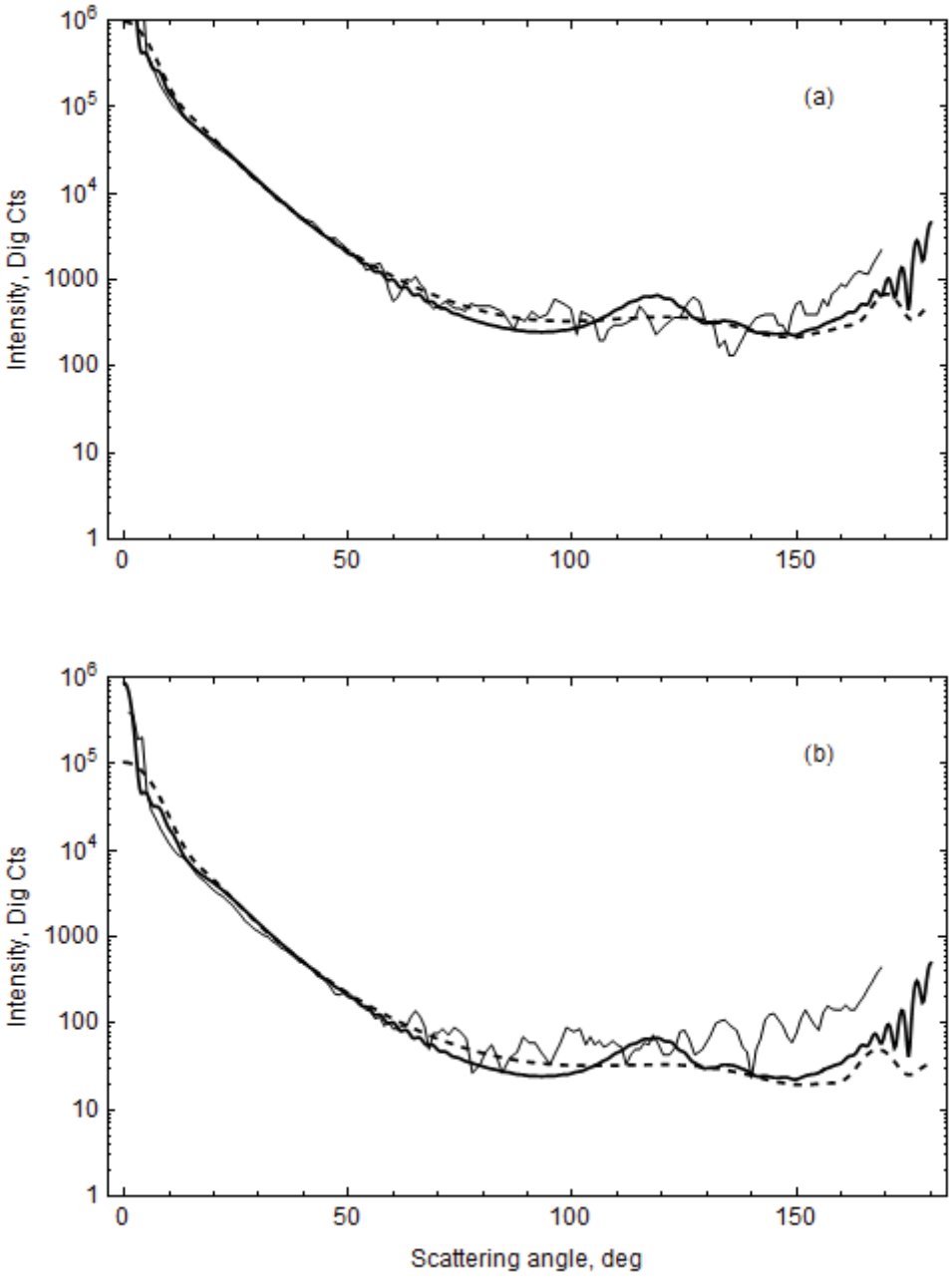
(a)
(b)
Intensity, Dig Cts
Intensity, Dig Cts
Scattering angle, deg
10^6
10^5
10^4
1000
100
10
1
0
50
100
150

Figure 7

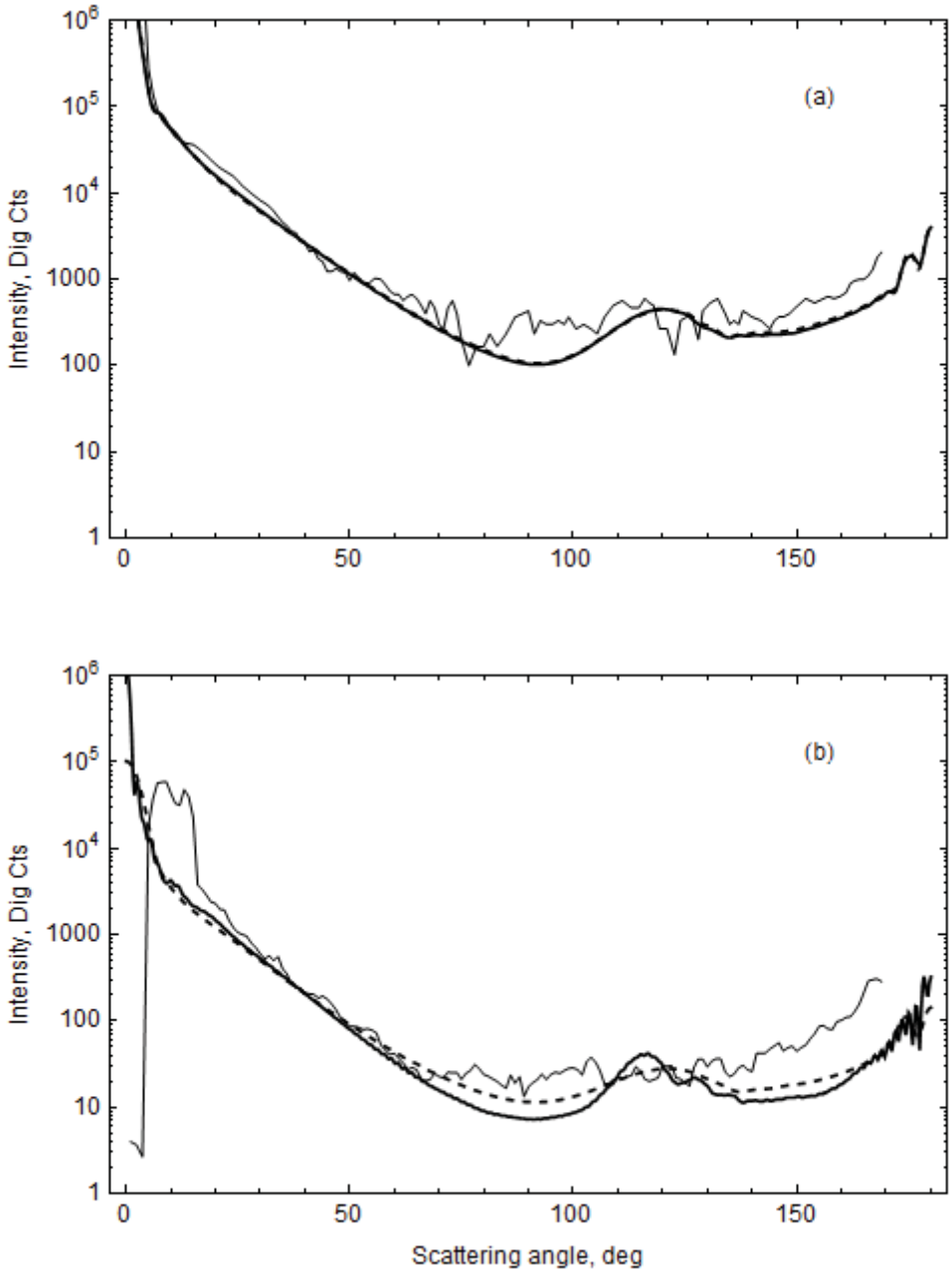
(a)
(b)
Intensity, Dig Cts
Scattering angle, deg
10^6
10^5
10^4
1000
100
10
1
0
50
100
150

Figure 8

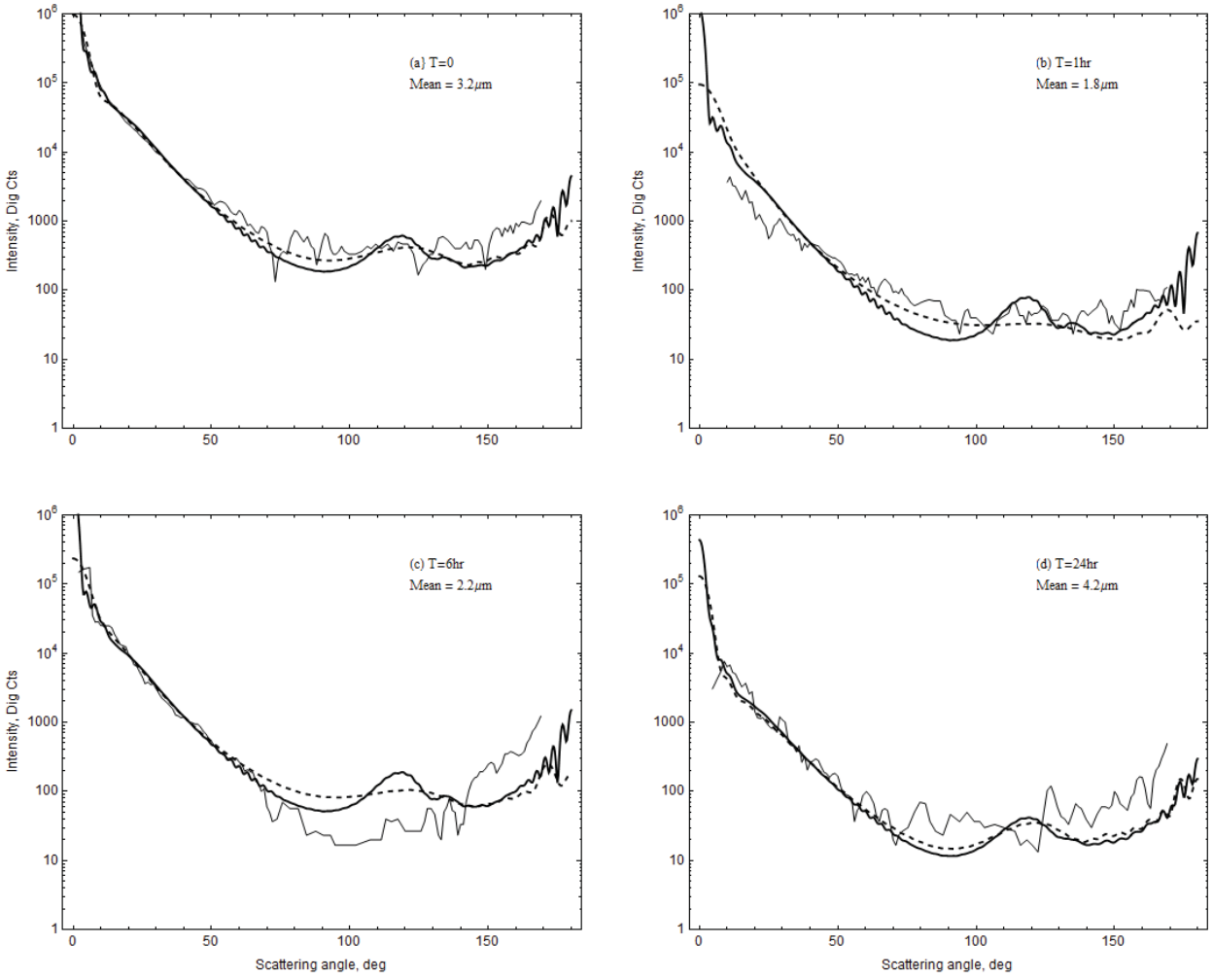
(a) T=0
Mean = 3.2μm
(b) T=1hr
Mean = 1.8μm
(c) T=6hr
Mean = 2.2μm
(d) T=24hr
Mean = 4.2μm
Intensity, Dig Cts
Scattering angle, deg

Figure 9